Graphical Abstract

885 °C

930 °C

2 µm

Nano-SIMS mapping of chlorine

(a) (b) (c)

● Co
● Cl

Atom Probe tomography

Impact of temperature on chlorine contamination and segregation for Ti(C,N) CVD thin hard coating studied by Nano-SIMS and Atom Probe Tomography.

Idriss El Azhari [a,b*], Jenifer Barrirero [a], Nathalie Valle [c], José García [d], Linus von Fieandt [d], Michael Engstler [a], Flavio Soldera [a], Luis Llanes [b], Frank Mücklich [a]

[a] Chair of Functional Materials, Department of Materials Science, Saarland University, Campus D 3.3, D-66123 Saarbrücken, Germany

[b] CIEFMA - Department of Materials Science and Engineering, EEBE – Campus Diagonal Besòs, Universitat Politècnica de Catalunya - BarcelonaTech, 08019 Barcelona, Spain

[c] Materials Research and Technology Department, Luxembourg Institute of Science and Technology, 41 rue du Brill, 4422 Belvaux, Luxembourg

[d] AB Sandvik Coromant R&D, Lerkrogsvägen 19, SE-126 80 Stockholm, Sweden

*Corresponding author: idriss.elazhari@uni-saarland.de

Abstract

High resolution characterization by Atom Probe Tomography (APT) and Secondary Ion Mass Spectrometry (SIMS) imaging were combined to highlight the nature of chlorine contamination and impact of deposition temperature for chemical vapor deposited Ti(C,N) thin

hard coating. It is highlighted that chlorine is spread and segregates exclusively at the grain boundaries. With increasing temperature (at 930°C), columnar grains of Ti(C,N) become coarser and chlorine segregation at the grain boundaries is reduced about 3 times in comparison to lower temperature (at 885 °C). It also appears that the chlorine is less homogeneously distributed with chlorine rich/free regions as it is demonstrated by the powerful combination of nano-SIMS and APT which gave a great insight of the spatial distribution of segregating elements at grain boundaries at nano- and micrometric scales.

Keywords

Ti(C,N) thin hard coating, Chemical Vapor Deposition, Grain boundary segregation, High-resolution Secondary Ion Mass Spectrometry (SIMS) imaging, APT.

Transition metal carbides, nitrides and carbonitrides are used in a wide range of technological applications [1–6]. The concern or awareness of the decisive role of the chemistry, nature and structure of grain boundaries (GBs) has been increasing through the years to the point that grain boundary engineering is becoming one of the most exciting routes to significantly tailor the physical properties of materials. Tailoring of grain boundary segregation is emerging as an interesting microstructural design approach due to the observations that solutes (or impurities) in very small amounts can greatly tune the structure, phase state and atomic bonding [7]. Segregation/contamination of chlorine in thin films can either enhance the semi-conducting properties in photovoltaic applications [8,9] or degrade the mechanical properties for wear-resistant hard coatings [10–12]. In this respect, the authors have demonstrated earlier with atom probe tomography (APT) for the first time that chlorine contamination is actually present in the form of segregation at the GBs in Ti(C,N), even at temperatures close to 885°C. Besides, unlike Zr(C,N), this exclusive chlorine segregation at

2

the GBs is correlated to the embrittlement of GBs and pure intergranular fracture during failure for Ti(C,N) [10–12]. APT has the advantage of revealing the three-dimensional distribution of chlorine at the GBs with near atomic resolution. However, the volumes imaged are small, what makes the analysis very localized. Other analytical techniques are required for a better insight of the areal/surface distribution of the chlorine contamination. For this purpose, the first objective of the present work is to investigate the chlorine contamination distribution for a wider field of view by using high-resolution Secondary Ion Mass Spectrometry (nano-SIMS) imaging to check if the segregation is local or widespread across the sample. In the literature, it is established that chlorine contamination decreases with rising deposition temperature [13–24], which is one of the principal factors that influence the chlorine contamination in CVD processes. Therefore, a second objective is to evaluate the impact of increasing deposition temperature on chlorine contamination/segregation. Then chlorine contamination distribution for Ti(C,N) coating deposited at higher temperature will be investigated and compared by combination of APT and nano-SIMS.

Two sets of Ti(C,N) coatings were deposited using moderate temperature CVD process (MT-CVD) in an industrial hot wall reactor using mainly titanium tetrachloride (TiCl$_4$), acetonitrile (CH$_3$CN) and hydrogen (H$_2$) precursors. Nitrogen (N$_2$) and Hydrogen chloride (HCl) were added to the reactor for thickness homogeneity. The substrate is a fine grade WC-6wt%Co cemented carbide. TiN starting interlayer was first deposited on the substrate to promote nucleation and growth of the coating [25]. Each set of samples was deposited at two different constant temperatures, 885 °C (Ti(C,N) $^{885\ °C}$) and 930 °C (Ti(C,N) $^{930\ °C}$) while maintaining all other deposition parameters unchanged for both depositions.

APT samples were extracted from an embedded cross section of the coating. The growth direction of the coating is perpendicular to the main axis (Z) of the reconstruction as previously described in [11]. Samples' lift-out and preparation were carried out in a dual-beam focused

ion beam/scanning electron microscope workstation (FIB/SEM) Helios NanoLab 600™ (FEI) following the procedure in [26]. After thinning the specimens, a low energy milling at 2 kV was performed to minimize gallium induced damage. APT was carried out in a LEAP 3000X HR (CAMECA) in laser mode. All measurements were performed at repetition rate of 200 kHz, pressure lower than 1.33×10^{-8} Pa, and evaporation rate of 5 atoms per 1000 pulses. Laser-pulsed APT was accomplished using a laser with a wavelength of 532 nm, pulse length of 10 ps, and a pulse energy of 0.5 nJ while keeping a specimen temperature of about 50-60 K. Datasets were reconstructed and analyzed with IVAS™3.6.14 software (CAMECA) based on the voltage curves. The evaporation field was estimated to be 40 V/nm. This estimation was done with the help of the Kingham curves for Ti [27]. All specimens were reconstructed with an image compression factor of 1.65 and a k-factor of 3.3 [28].Compositions were obtained after background subtraction and applying a peak-decomposition analysis in IVAS software. Because of the high amount of molecular ions and multiple events during acquisition, two methods presented in literature were applied to correct the C content in the coatings: ^{13}C-method [29] and 24 Da peak correction [30].

For the nano-SIMS analysis, a mirror-polished plain surface (down to 0.02 μm alumina polishing suspension as the final step) of the coating was prepared simultaneously for both sets of samples in the same embedding (Bakelite resin). The nano-SIMS maps were performed perpendicularly to the growth direction of the coating. Identical preparation is made for both samples. Hence, the same amount of material is removed for both samples during polishing which makes the comparison and analysis reliable as the measurements are carried out at the same depth below the sample top surface. Nano-SIMS characterization for both samples was made during the same campaign of measurement. The analyses have been carried out on a CAMECA NanoSIMS instrument in imaging mode with a Cs^+ primary ion beam to sputter the material. Negative polarization was applied to collect the negative Cl^- ions. One set of images includes maps recorded simultaneously for the following negative ions: ^{12}C, ^{18}O, ^{12}C^{14}N, ^{35}Cl and ^{48}Ti^{12}C.

Images from Nano-SIMS measurements were binarized and the grain boundaries were reconstructed using a watershed algorithm with software package a4i analysis from aquinto [31]. The 3D surface density S_V has been calculated from the specific line length L_A in the 2D image according to relation $S_V = 4/\pi * L_A$ [32].
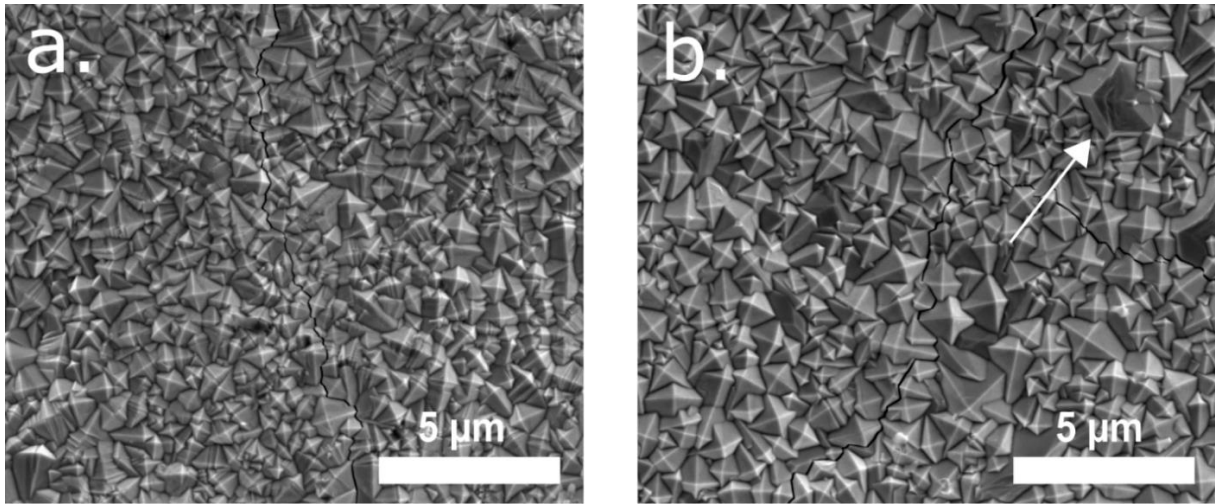
Fig. 1 Plain surface secondary electrons SEM images of Ti(C,N) deposited at (a) 885 °C and (b) 930 °C. CVD cooling cracks are seen for both samples. Coarse star-shaped crystals (white arrow) appear exclusively for 930 °C.

Fig. 1 shows the topography after deposition for both Ti(C,N) [885 °C] and Ti(C,N) [930 °C]. Mainly columnar pyramidal faceted crystals are present for both samples with a coarser grain size distribution for Ti(C,N) [930 °C] (diameter mean value for Ti(C,N) [885 °C] and Ti(C,N) [930 °C] are 0.58±0.2 and 0.86±0.25 µm, respectively). Besides, star-shaped crystals are present only for Ti(C,N) [930 °C.]. CVD cooling cracks, induced by the difference of the coefficient of thermal expansion between coating and substrate, are present in both samples, and they mostly propagate through the grain boundaries. This crack extension mode was highlighted at different test scales by micropillar compression [10] and spherical indentation [12] which highlights that the brittleness at GBs is rather intrinsic. This result has been mainly attributed to the segregation of chlorine at grain boundaries for Ti(C,N) [885 °C] in comparison to Zr(C,N) [11].

5

Table 1 confirms the same overall concentrations measured by APT for the Ti(C,N) coatings at both deposition temperatures. The composition for each coating was calculated as the average composition of five grains (without including GBs) weighted by the number of counts analyzed in each grain. The standard deviations reported show the deviation in the compositions of the five grains and it was weighted by the number of counts in each analysis as well. This result suggests that there is a slightly larger fluctuation in Ti, C and N compositions between different grains for the coating grown at a higher temperature. Figure 2 shows an APT reconstruction evidencing the chlorine contamination in Ti(C,N) $^{930\ °C}$. Chlorine and cobalt segregate separately at the grain boundaries for the high temperature sample with small islands of chlorine demixed in cobalt. Cobalt diffuses from the substrate at high temperature during the deposition. Concentration profiles (in cylindrical regions) in Cl-rich regions show that, similarly to the results of Ti(C,N) $^{885\ °C}$, there is a slight increase of titanium concentration with a decrease in C and N. As reported previously by the authors [11], this could support that chlorine segregate as titanium sub-chlorides instead of pure chlorine. However, due to the slight change in concentration, no clear trend for Ti can be seen at the boundary when considering the Ti cumulative curves. The change in structure and composition at grain boundaries produces local variations in the evaporation field during an APT measurement. This variation may affect the trajectory of atoms near the boundary and the mass spectrum. Considering this and the overlap of Ti and C at 24 Da in the present analysis, the evaluation of the Ti content at the boundary is extremely challenging.

The cobalt and chlorine interfacial excess at the grain boundaries in Ti(C,N) coatings deposited at 885 °C and 930 °C were calculated from the slope of cumulative diagrams constructed based on concentration profiles across the grain boundaries as shown in Fig. 2 (d,e,f,g). Ten profiles were constructed and calculated for each sample: five of them at Co-rich regions and five at Cl-rich regions. The cobalt ranges of concentration at the grain boundaries vary between 1.7 at.% – 3.3 at.% for Ti(C,N) $^{885\ °C}$ and 2.2 at.% – 6.3 at.% for Ti(C,N) $^{930\ °C}$. This finding confirms a higher range of concentrations of cobalt at the grain boundaries of the

6

sample manufactured at higher temperature. This is a natural consequence of the increased cobalt diffusion at a higher temperature. On the contrary, when considering the trend of chlorine at the boundary, the concentration ranges vary between 1.5 at. % – 2.6 at.% for Ti(C,N) [885 °C] and 1.4 at.% – 1.9 at.% for Ti(C,N) [930 °C]. Interestingly, chlorine concentration shows the opposite trend than cobalt, with a slightly lower concentration of chlorine at the boundaries of the sample manufactured at higher temperature. It needs to be taken into account that the concentrations at the grain boundaries depend on the type of boundary and the crystal orientation of the grains. This is not considered here in detail, but instead the aim of the measurements is to get an overall comparison of the segregations at the boundaries. Regarding the overall concentration, the C:N stoichiometry of about 1.2 correlates to similar coatings characterized by X-ray photoelectron spectroscopy (XPS) [33,34]. This result supports that the measured C and N concentrations are accurate and might not be totally attributed to the shortcomings of the APT characterization discussed in [11,35].

Table 1: APT overall composition comparison between Ti(C,N) [930 °C] and Ti(C,N) [885 °C].

Sample	Ti	C	N	O	Cl	Co
930 °C	51.8 ± 1.4	26.2 ± 2.1	21.8 ± 0.7	0.09 ± 0.01	0.02 ± 0.01	0.03 ± 0.01
885 °C	51.6 ± 0.4	26.2 ± 0.6	22.0 ± 0.4	0.16 ± 0.06	0.02 ± 0.01	0.06 ± 0.02

From the reconstruction in Fig. 2, it appears that oppositely to cobalt, chlorine segregation is isolated in small islands with inhomogeneous distribution. Due to the restricted volumes imaged by APT, nano-SIMS was used as a complement to image a wider field of view.
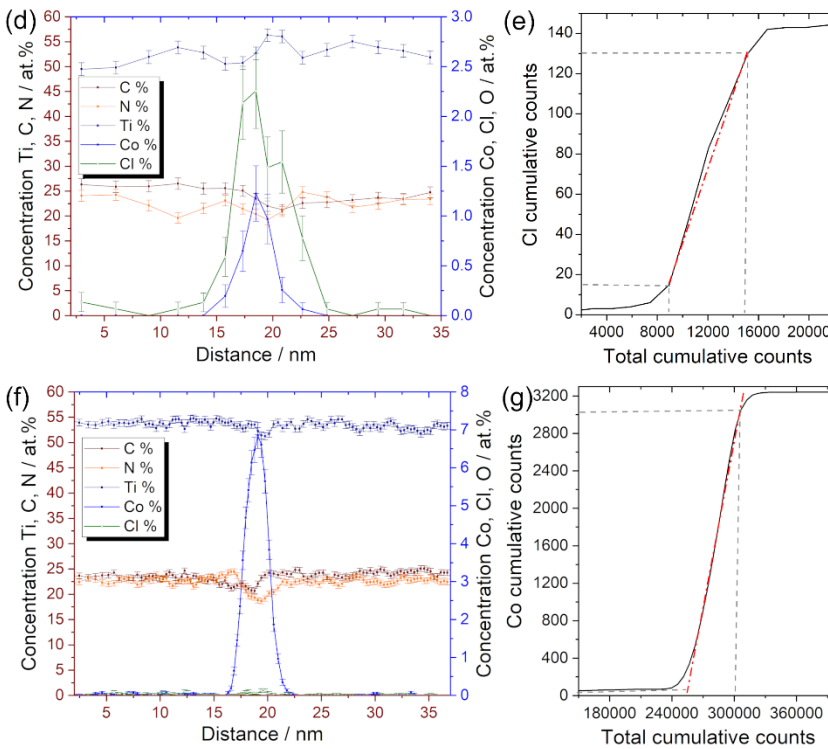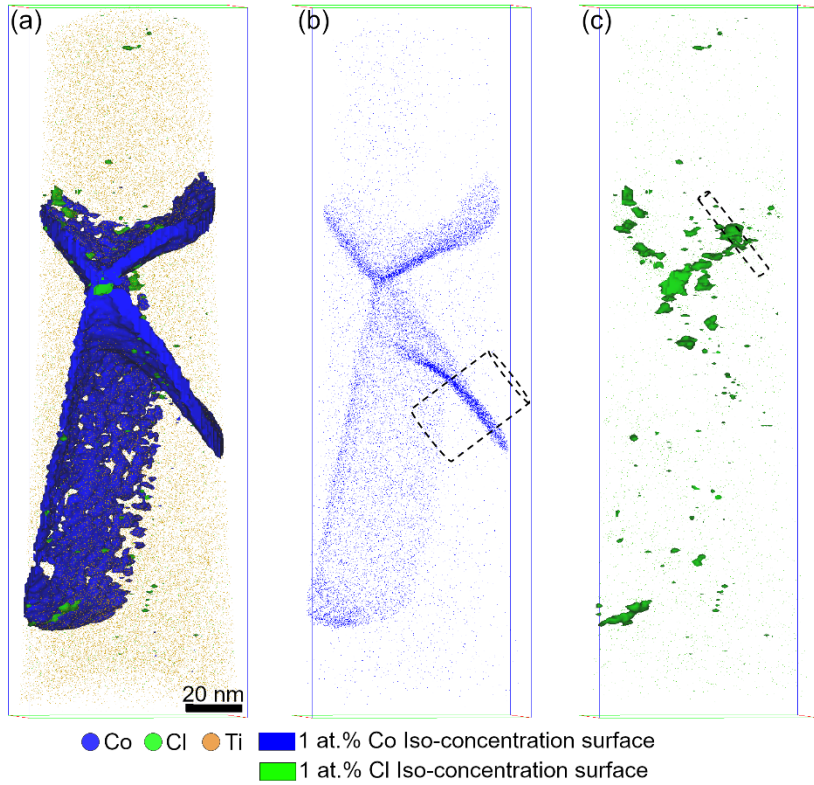
Fig. 2: APT reconstructions of Ti(C,N) $^{930\ °C}$ (a) Highlight of the segregation at the grain boundaries by 1 at.% Iso-concentration surfaces of Cl and Co (b) distribution of Co atoms represented as small spheres. The cylinder shows the position of the concentration profile (c) distribution of Cl atoms represented as small spheres with 1 at.% Iso-concentration surfaces of Cl to highlight the small islands containing Cl at the boundary. The cylinder shows the position of the concentration profile. (d,f) Concentration profiles across Cl and Co-rich regions (e,g) corresponding cumulative diagram constructed from (d,f), respectively. The growth direction of the coating is perpendicular to the longer axis of the reconstruction.

8

High-resolution SIMS mapping of chemical elements (C, O, CN, Cl, and TiC) with nano-SIMS is shown in Fig. 3. Lower counts for TiC$^-$ (which is used to track titanium) ion are discerned, as compared to other ions due to the higher ionization energy of this compound. The compound CN- has a high electron affinity (3.86 eV from [36]). As a consequence, the ionization of CN$^-$ is relatively high what provides an orientation contrast image of the different crystals. C and N occupy octahedral interstices in a B1 structure, and the different crystallographic planes have different atomic density. Then, the sputtering or ionization is influenced by the orientation of the crystals. The correlation between the crystal orientation and SIMS CN$^-$ intensities is out of the scope of the present work. Nevertheless, this result can support that C and N have random distribution in interstitial planes as it has been suggested by other authors [37].

9
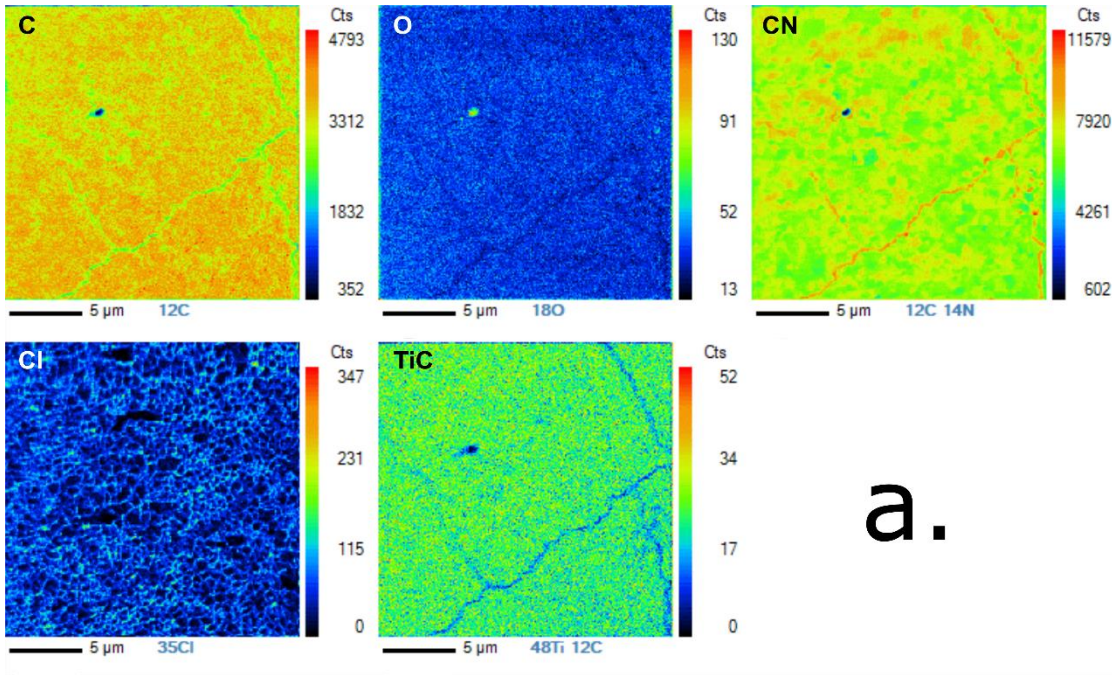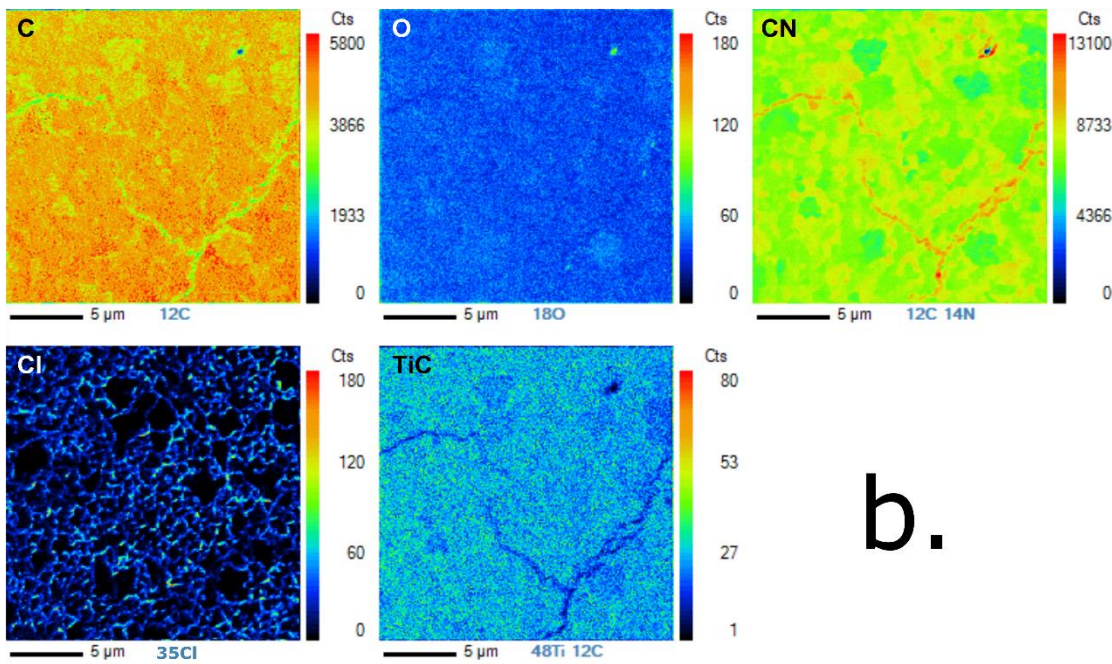
Fig. 3: Plain surface elements mapping of ^{12}C, ^{18}O, $^{12}C^{14}N$, ^{35}Cl and $^{48}Ti^{12}C$ for (a) Ti(C,N) $^{885\ °C}$ and (b) Ti(C,N) $^{930\ °C}$ with nano-SIMS. Acquisition time 30 ms/pixel; Field of view (20×20) µm². Image size (256×256) pixels. Linear scale. CVD cooling cracks appears clearly in the mapping of CN and TiC and C Mapping is perpendicular to the growth direction of the coating.

Chlorine mapping reveals that this element segregates broadly and exclusively at the grain boundaries for both Ti(C,N) $^{885\ °C}$ and Ti(C,N) $^{930\ °C}$ which endorses and confirms previous APT results obtained by the authors and discards the assumption [14,19,21,22,38–42] that chlorine forms a solid solution with Ti, C and N. However, it seems that there are peaks of chlorine

10

concentration which are more pronounced for Ti(C,N) [930 °C], in contrast to Ti(C,N) [885 °C], with the presence of boundaries more enriched than others. This correlates with the corresponding APT reconstructions (Fig. 2), where dispersed Cl clusters are seen for Ti(C,N) [930 °C]. For Ti(C,N) [885 °C], chlorine segregates at the grain boundaries as well with a finer structure due to the smaller grain size. From Fig. 4 we can see that the number of counts which is an indication of concentration is largely higher for Ti(C,N) [885 °C]. Mapping of chlorine with nano-SIMS shows to form a continuous concentration line at the GBs due the lower spatial resolution limit - in comparison to APT - estimated to be 50 nm. To compare quantitatively chlorine concentration at grain boundaries, chlorine levels were compared in samples Ti(C,N) [885 °C] and Ti(C,N) [930 °C] by summing up the intensity of Cl^- over 4-5 random areas of (10 × 10) μm^2 and (20 × 20) μm^2, then normalizing it to the signal of TiC. A ratio $I(Cl)_{norm\ 885\ °C}$ / $I(Cl)_{norm\ 930\ °C}$ of about 4.5 was obtained, indicating a higher chlorine concentration for Ti(C,N) [885 °C] sample. Nevertheless, as the grain size is finer for Ti(C,N) [885 °C], the GBs length should be normalized to get the correct comparison between samples. The grain boundaries length was calculated by image analysis with A4i software [31], and it was found out that it decreased by 24% for Ti(C,N) [930 °C] compared to Ti(C,N) [885 °C] . As a result, by taking into consideration the decrease of GBs length of about 24% for Ti(C,N) [930 °C], chlorine concentration is reduced around 3.4 times.
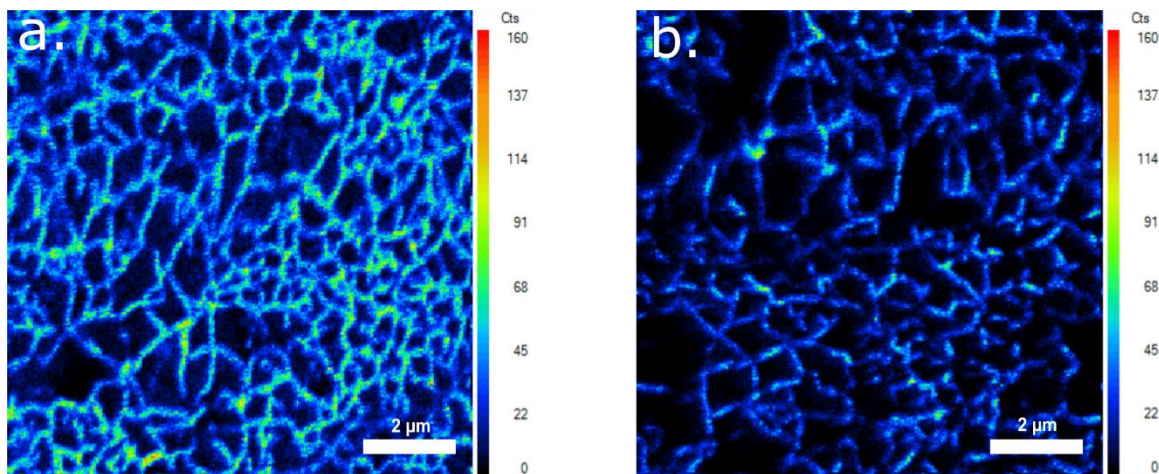
Fig. 4: Chlorine mapping comparison for (a) Ti(C,N) [885 °C] and for (b) Ti(C,N) [930 °C]. Lower concentration and less homogeneity of chlorine segregation at the GBs can be seen with the temperature increase (mapping is perpendicular to the growth direction of the coating).

First of all, it is important to highlight that the reported literature about chlorine contamination concerns CVD processes at relatively lower temperatures, i.e. less than 885 – 930 °C. For TiN CVD processes using titanium chloride as a precursor, chlorine contamination/impurities have been reported to be incorporated in the crystal lattice [14,19,21,22,38–42] or segregated at the grain boundaries [15,16]. However, no direct evidence was yet provided; thus, controversy cannot be settled. Due to the small volume imaged by APT and restricted number of the analyzed specimens, the present results with nano-SIMS validate and complement the previous work of the authors and provide a strong evidence. Chlorine contamination in the form of segregation at the grain boundaries exists even at the deposition temperature range of 885 – 930 °C. This concerns at least moderate temperature CVD processes. It is well known in the literature that chlorine contamination is reduced with increasing temperature [13–24]. The nano-SIMS investigations have highlighted quantitatively that the chlorine segregation at the GBs is reduced about 3.4 times. Moreover, the distribution of chlorine is kind of discontinuous (or relatively less homogeneous) with the appearance of isolated maximum concentration peaks when increasing the temperature, as it can be seen in Fig. 3 and Fig. 4. At very high temperatures, the thermal dissociation of $TiCl_4$ precursor to subchloride ($TiCl_x$) is difficult [43]. Chlorine reduction is mainly attributed to the reaction with H_2 and formation of HCl which is the most stable form of chlorine [44]. Then, the decrease of chlorine (or desorption reaction) with temperature is attributed to the enhanced formation of HCl, which could explain the lower and less homogeneous segregation distribution of chlorine. The decreased residence time/sticking coefficient of the precursors with temperature rise [45] could be also responsible behind the lower chlorine segregation. Nucleation and growth of CVD thin films is a very complex field due to its atomistic nature [46]. The increase of temperature is affecting many interacting factors that are directly related to nucleation and growth [46]. It was reported that grain size increases with lower chlorine contamination - which is related to deposition temperature – for Ti(C,N) [18,19] and TiN [22]. The increase of grain size accompanied with the decrease of chlorine segregation might be

12

connected/related as it is suggested that chlorine adsorbs at crystal facets during growth limiting the grain size [22]. More generally chlorine segregation could be considered as a structure/microstructure forming mechanism of a thin coating [47] which means that chlorine affects the microstructure/morphology of the coating [19]. In this sense, new distributed star-shaped crystals (which are very similar fivefold symmetry crystals) are seen only for the high temperature sample. Explaining the appearance of these crystals by increasing the deposition temperature is out of scope of the present study. The star shaped crystals appear exclusively by increasing the temperature which can be related to several factors that are induced by temperature rise. It was reported by several authors that increase of temperature is promoting the appearance of these crystal shapes for Ti(C,N) [48,49] and TiN [50,51]. Further investigations should be carried out in order to establish a direct causality or link which is again out of scope of the present investigation.

In summary, the combination of high-resolution characterization techniques with APT and nano-SIMS, has been shown to be complementary and quite effective approach to provide a direct and strong evidence of the spatial distribution at the near atomic and micrometric scales of the segregating elements at grain boundaries. Nano-SIMS characterization has yielded a direct proof of spread segregation of chlorine exclusively at the GBs of Ti(C,N) deposited through moderate temperature process at 885 °C and 930 °C. It permits to confirm former results obtained by means of APT by the authors. With an increase of 45 °C above 885 °C, grain size increased and it appears that chlorine segregation is less homogeneous with appearance of isolated chlorine peaks: small clusters of chlorine within the diffused cobalt are seen with APT and chlorine rich zones are highlighted by nano-SIMS. It is estimated by nano-SIMS that the chlorine concentration is 3.4 times lower for Ti(C,N) deposited at 930 °C.

Acknowledgement

References

[1]   S. Piscanec, Acta Mater. 52 (2004) 1237–1245.

[2]   S. DelaCruz, Z. Wang, P. Cheng, C. Carraro, R. Maboudian, Thin Solid Films 670 (2019) 54–59.

[3]   P. Patsalas, N. Kalfagiannis, S. Kassavetis, Materials 8 (2015) 3128–3154.

[4]   Y. Zhong, X. Xia, F. Shi, J. Zhan, J. Tu, H.J. Fan, Adv. Sci. 3 (2016) 1500286.

[5]   W.G. Fahrenholtz, G.E. Hilmas, Scr. Mater. 129 (2017) 94–99.

[6]   K. Bobzin, CIRP J. Manuf. Sci. Technol. 18 (2017) 1–9.

[7]   D. Raabe, M. Herbig, S. Sandlöbes, Y. Li, D. Tytko, M. Kuzmina, D. Ponge, P.-P. Choi, Curr. Opin. Solid State Mater. Sci. 18 (2014) 253–261.

[8]   S.P. Harvey, G. Teeter, H. Moutinho, M.M. Al-Jassim, Prog. Photovolt. Res. Appl. 23 (2015) 838–846.

[9]   J.D. Major, M. Al Turkestani, L. Bowen, M. Brossard, C. Li, P. Lagoudakis, S.J. Pennycook, L.J. Phillips, R.E. Treharne, K. Durose, Nat. Commun. 7 (2016) 13231.

[10] I. El Azhari, J. Garcia, M. Zamanzade, F. Soldera, C. Pauly, L. Llanes, F. Mücklich, Acta Mater. 149 (2018) 364–376.

[11] I. El Azhari, J. Barrirero, J. García, F. Soldera, L. Llanes, F. Mücklich, Scr. Mater. 162 (2019) 335–340.

[12] I. El Azhari, J. García, F. Soldera, S. Suarez, E. Jiménez-Piqué, F. Mücklich, L. Llanes, Int. J. Refract. Met. Hard Mater. 86 (2020) 105050.

[13] S.R. Kurtz, R.G. Gordon, Thin Solid Films 140 (1986) 277–290.

[14] T. Arai, H. Fujita, K. Oguri, Thin Solid Films 165 (1988) 139–148.

[15] M.J. Buiting, A.H. Reader, MRS Online Proc. Libr. Arch. 168 (1989).

[16] M.J. Buiting, A.F. Otterloo, A.H. Montree, J. Electrochem. Soc. 138 (1991) 500–505.

[17] N. Yokoyama, J. Electrochem. Soc. 138 (1991) 190–195.

[18] S.B. Kim, S.K. Choi, S.S. Chun, K.H. Kim, J. Vac. Sci. Technol. Vac. Surf. Films 9 (1991) 2174–2179.

[19] B. Arnold, I. Endler, Microchim. Acta 125 (1997) 83–87.

[20] N. Ramanuja, R.A. Levy, S.N. Dharmadhikari, E. Ramos, C.W. Pearce, S.C. Menasian, P.C. Schamberger, C.C. Collins, Mater. Lett. 57 (2002) 261–269.

[21] K. Kawata, H. Sugimura, O. Takai, Thin Solid Films 407 (2002) 38–44.

[22] M. Stoiber, E. Badisch, C. Lugmair, C. Mitterer, Surf. Coat. Technol. 163–164 (2002) 451–456.

[23] E. Badisch, C. Mitterer, P.H. Mayrhofer, G. Mori, R.J. Bakker, J. Brenner, H. Störi, Thin Solid Films 460 (2004) 125–132.

[24] J. Wagner, V. Edlmayr, M. Penoy, C. Michotte, C. Mitterer, M. Kathrein, Int. J. Refract. Met. Hard Mater. 26 (2008) 563–568.

[25] I. El Azhari, J. García, M. Zamanzade, F. Soldera, C. Pauly, C. Motz, L. Llanes, F. Mücklich, Mater. Des. 186 (2020) 108283.

[26] K. Thompson, D. Lawrence, D.J. Larson, J.D. Olson, T.F. Kelly, B. Gorman, Ultramicroscopy 107 (2007) 131–139.

[27] D.R. Kingham, Surf. Sci. 116 (1982) 273–301.

[28] P. Bas, A. Bostel, B. Deconihout, D. Blavette, Appl. Surf. Sci. 87–88 (1995) 298–304.

[29] M. Thuvander, J. Weidow, J. Angseryd, L.K.L. Falk, F. Liu, M. Sonestedt, K. Stiller, H.-O. Andrén, Ultramicroscopy 111 (2011) 604–608.

[30] J. Angseryd, F. Liu, H.-O. Andrén, S.S.A. Gerstl, M. Thuvander, Ultramicroscopy 111 (2011) 609–614.

[31] A. Velichko, Quantitative 3D Characterization of Graphite Morphologies in Cast Iron Using FIB Microstructure Tomography, Universität des Saarlandes, 2008.

[32] J.C. Russ, R.T. Dehoff, Practical Stereology, Springer US, Boston, MA, 2000.

[33] L. von Fieandt, K. Johansson, T. Larsson, M. Boman, E. Lindahl, Thin Solid Films 645 (2018) 19–26.

[34] L. von Fieandt, T. Larsson, M. Boman, E. Lindahl, J. Cryst. Growth 508 (2019) 90–95.

[35] I. Povstugar, P.-P. Choi, D. Tytko, J.-P. Ahn, D. Raabe, Acta Mater. 61 (2013) 7534–7542.

[36] S.E. Bradforth, E.H. Kim, D.W. Arnold, D.M. Neumark, J. Chem. Phys. 98 (1993) 800–810.

[37] G. Levi, W.D. Kaplan, M. Bamberger, Mater. Lett. 35 (1998) 344–350.

[38] R. Leutenecker, B. Fröschle, U. Cao-Minh, P. Ramm, Thin Solid Films 270 (1995) 621–626.

[39] S. Li, W. Huang, H. Yang, Z. Wang, Plasma Chem. Plasma Process. 4 (1984) 147–161.

[40] K.-T. Rie, A. Gebauer, J. Woehle, Surf. Coat. Technol. 60 (1993) 385–388.

[41] K.-T. Rie, A. Gebauer, J. Wöhle, Surf. Coat. Technol. 86 (1996) 498–506.

[42] K. Wetzig, I. Endler, Microchim. Acta 125 (1997) 121–125.

[43] F. Teyssandier, J. Electrochem. Soc. 145 (1998) 2167.

[44] K.H. Kim, S.H. Lee, Thin Solid Films 283 (1996) 165–170.

[45] P. Stenberg, P. Sukkaew, I. Farkas, O. Kordina, E. Janzén, L. Ojamäe, Ö. Danielsson, H. Pedersen, J. Phys. Chem. C 121 (2017) 2711–2720.

[46] F. Teyssandier, A. Dollet, in: Pergamon Mater. Ser., Elsevier, 1999, pp. 257–285.

[47] P.B. Barna, M. Adamik, Thin Solid Films 317 (1998) 27–33.

[48] J. Garcia, R. Pitonak, R. Weissenbacher, A. Köpf, Surf. Coat. Technol. 205 (2010) 2322–2327.

[49] J. Garcia, R. Pitonak, L. Agudo, A. Kostka, Mater. Lett. 68 (2012) 71–74.

[50] H.-E. Cheng, M.-H. Hon, J. Cryst. Growth 142 (1994) 117–123.

[51] H.-E. Cheng, Y.-W. Wen, Surf. Coat. Technol. 179 (2004) 103–109.

1
2
3
4
5
6
7
8
9
10
11
12
13
14
15
16
17
18
19
20
21
22
23
24
25
26
27
28
29
30
31
32
33
34
35
36
37
38
39
40
41
42
43
44
45
46
47
48
49
50
51
52
53
54
55
56
57
58
59
60
61
62
63
64
65

Declaration of interests

☒ The authors declare that they have no known competing financial interests or personal relationships that could have appeared to influence the work reported in this paper.

☐The authors declare the following financial interests/personal relationships which may be considered as potential competing interests:

Idriss El Azhari, Jenifer Barrirero, Nathalie Valle, José García, Linus von Fieandt, Michael Engstler, Flavio Soldera, Luis Llanes, Frank Mücklich